Alexandria Engineering Journal (2012) **51**, 153–169

Alexandria University

Alexandria Engineering Journal

www.elsevier.com/locate/aej
www.sciencedirect.com

ORIGINAL ARTICLE

Comparative investigation of the stagger variation influence on the hydrodynamic interference of high speed trimaran

K.A. Hafez *, A.A. El-Kot

Department of Naval Architecture and Marine Engineering, Faculty of Engineering, Alexandria University, Alexandria, Egypt

Received 22 June 2011; revised 13 December 2011; accepted 5 February 2012
Available online 3 March 2012

KEYWORDS

High speed trimaran (HST);
Hydrodynamic interference factor (HIF);
Calm water resistance of trimaran;
Stagger of outriggers;
Wigley©-st model;
AMECRC©-09 model;
NPL©-4a model

Abstract This paper numerically investigates the influence of stagger variation of the outriggers on the hydrodynamic interference of high speed trimaran (HST). The slender body method (SBM) embedded in the Hullspeed© [1] module of the Maxsurf© [2] package is used for calculating the resistance of three symmetric trimaran series moving in a calm free surface of deep water. Each individual trimaran series comprises of 4681 configurations generated by considering 151 staggers covering the interval ($-50\% \leqslant \alpha \leqslant +100\%$), and 31 separations covering the interval ($100\% \leqslant \beta \leqslant 400\%$) for 81 Froude numbers covering the interval ($0.20 \leqslant F_n \leqslant 1.0$). In developing the three trimaran series, Wigley©-st [3], AMECRC©-09 [4,5], and NPL©-4a [6,7] models are used separately for both the main and side hulls of each individual series models. Seeking automation, a computer macro-named Tri-PL© is developed from scratch based on the Visual Basic for Applications© [8] programming language. To generate each model of the individual series together with its detailed hydrostatic particulars, Tri-PL© automatically interferes the Maxsurf© [2] module. To calculate the resistance components together with the associating wave pattern for each model of the individual series, Tri-PL© automatically interferes the Hullspeed© [1] module. To benchmark Tri-PL© macro-together with the mathematical procedures embedded therein, and to rely on the analysis outcomes, the numerical results of both Wigley©-st [3] and AMECRC©-09 [4,5] models are validated. To visualize the significant data of the analysis properly, a graph template of the SigmaPlot©

* Corresponding author. Tel.: +20 127 119 0633; fax: +20 3 592 1853.
E-mail address: kamhjp@lycos.com (K.A. Hafez).
Peer review under responsibility of Faculty of Engineering, Alexandrian University.

Production and hosting by Elsevier

http://dx.doi.org/10.1016/j.aej.2012.02.002

[9] is created to read the numerical results of the Tri-PL©, and then automatically prepares all the necessary analysis graphs.

1. Introduction

The rapid transit for maritime transportation vehicles satisfying the paradox of high cruising speed at low resistance for use in the military, commercial, and recreational purposes, enthusiasm many researchers to realize more practical solutions of such paradox. Practically, particular difficulties arise in the design of high speed maritime vehicles; in which a relatively large increase in their resistance naturally associates any speed increment. Such resistance increment, therefore, requires an increase in the vehicles propelling power, and consequently, the weight and size of the propulsion engine. As an unconventional solution of such difficulties, few researchers devoted their efforts to investigate the hydrodynamic performance of the newly developed maritime vehicles, e.g., trimaran.

A trimaran is a multi-slender-hulled vehicle, consisting of one long main central hull and two shorter symmetric or asymmetric wing hulls (outriggers) located on both sides of the main hull. Therefore, the outriggers work as fenders; decreasing the main hull transverse bulkheads, size and number of its decks, and provide the trimaran with excellent static and dynamic stabilities as well as amazing seakeeping characteristics [10]. The aforementioned configuration of the trimaran provides high length-to-breadth L_W/B_W ratio which decreases its wave making resistance. Also, the low length-to-draft L_W/d_m ratio of the trimaran allows it to access areas inaccessible to comparable mono-hulls of similar sizes. The previously conducted numerical and experimental researches proved that the trimaran configuration reduced the overall drag of the vehicle by up to 20% of the comparable mono-hull [11]. The main hull and outriggers may be arranged so that the vehicle generated waves destructively interfere, producing smaller waves and thereby reducing the energy dissipated in overcoming the wave-making resistance [12].

Efforts to numerically compute water resistance date back more than a decade ago; when the Australian mathematician [13] proposed an integral expression for its computation. Unequivocally, due to its rigorous mathematical manipulation and the associated ambiguous physical interpretation, the problem still not completely solved satisfactorily. The numerical prediction of water resistance approached meaningful results by the end of the 1990s, when the boundary element method (BEM) has become a standard tool in manipulating the water resistance [14–19]. Even then, problems remained with water viscosity, breaking waves and the fundamental realistic dilemma of an integrated water resistance or at least the hypothetical approach of mutually interfered and bonded resistance components, which separately necessitates a comprehensive approach for a completely satisfactory treatment.

Although, the overall resistance components against which the trimaran may be designed to withstand is as shown in Fig. 1, this research focuses only on the numerical investigation of the influence of stagger variation of the outriggers on the prediction of the trimaran calm water resistance (blocks of white backgrounds) using SBM. The later method calculates the resistance of a maritime vehicle based on the far-field wave system and is thus not so susceptible to the problems associating the near-field approximations. An important part of wave resistance is associated with the energy in the far-field waves caused by the vehicle. The wave elevation can be measured along longitudinal cuts parallel to the ship's track, and the associated wave resistance can be calculated by assuming small wave slopes. This is called wave pattern resistance, but it does not account for the fact that the wave slopes can be large or that the waves break near the ship. Also, the trimaran resistance is evaluated without the presence of the propulsion unit; i.e., it is defined as the force necessary to tow the trimaran in calm water with a constant velocity on a straight track.

Many of the today's high-speed vessels; whether under construction or in service have transom sterns of different configurations and extents. In fact, transom sterns violate simple hydrodynamic analysis because of the vague extent and shape of the free surface vertices created behind the vehicle. In principle, the pressure acting on the surface of the vertices is atmospheric, and that the flow separates from the transom tangentially. Proper analysis of the hydrodynamic problems associating transom sterns would require a full 3D treatment in which it would be necessary to iterate the geometric shape of this stern hollow, until the relevant kinematic and dynamic conditions are satisfied. This is not an easy task and very time consuming issue, given that some aspects of such geometry are highly nonlinear, and perhaps even intractable within the framework of the potential-flow theory. In particular, the closure of the stern hollow associated with a non-negligible spray and flow unsteadiness, appears to be a dramatic fluid problem. Such vague flow region referred to as a rooster tail because of the resultant spray pattern thrown into air. Few researchers have addressed this issue, attempting to throw light upon the flow separation problem associating the stern hollow, among those are [20–29].

2. Generated model series

The first critical step in this research is to select an appropriate hull forms upon which a realistic trimaran model may be configured. In this regard, three well known slender models namely Wigley©-st [3], AMECRC©-09 [4,5], and NPL©-4a [6,7] are used separately in developing both the main and side hulls of three symmetric trimaran series. Each series comprises of 4681 configurations generated by considering 151 staggers covering the interval $-50\% \leqslant \alpha \leqslant +100\%$, and 31 separations covering the interval $100\% \leqslant \beta \leqslant 400\%$ for 81 Froude numbers covering the interval $0.20 \leqslant F_n \leqslant 1.0$. Figs. 2–4 show the geometric configurations of the aforementioned parent models respectively. The name of each parent model is used for referencing the trimaran that is build-upon.

The principal particulars of the main and side hulls of each trimaran are tabulated in Table 1, in which the following

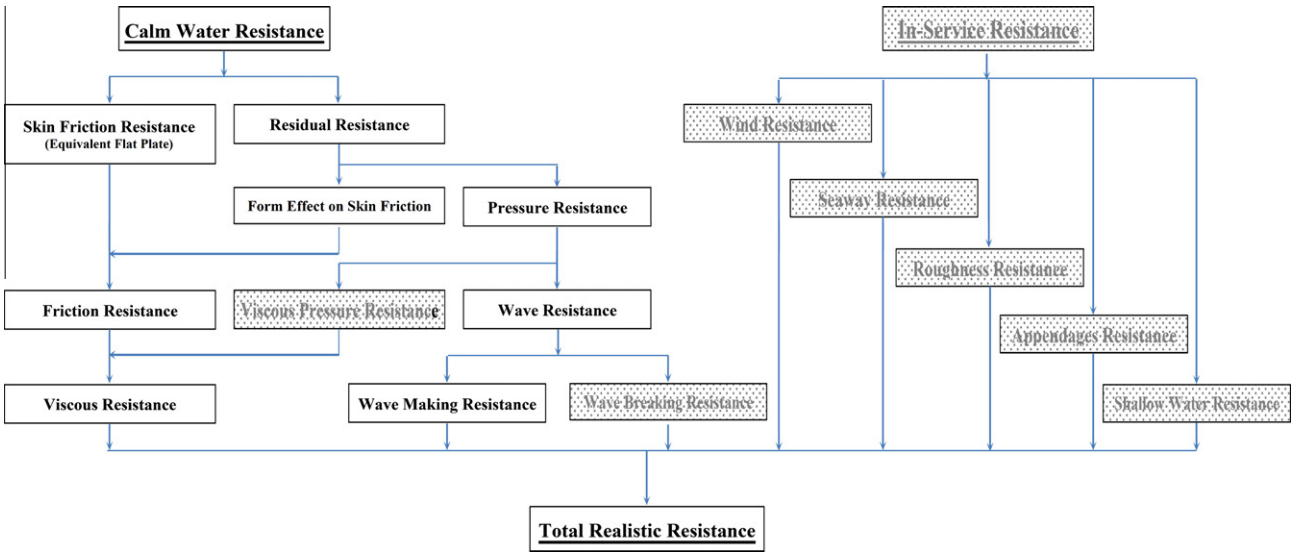

Figure 1 Components of calm water resistance.

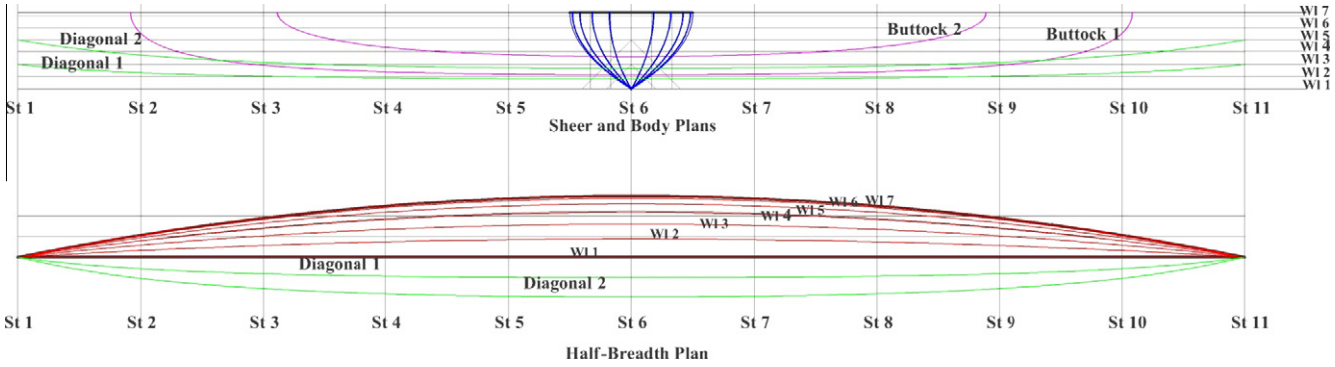

Figure 2 Wigley©-st parent model configuration.

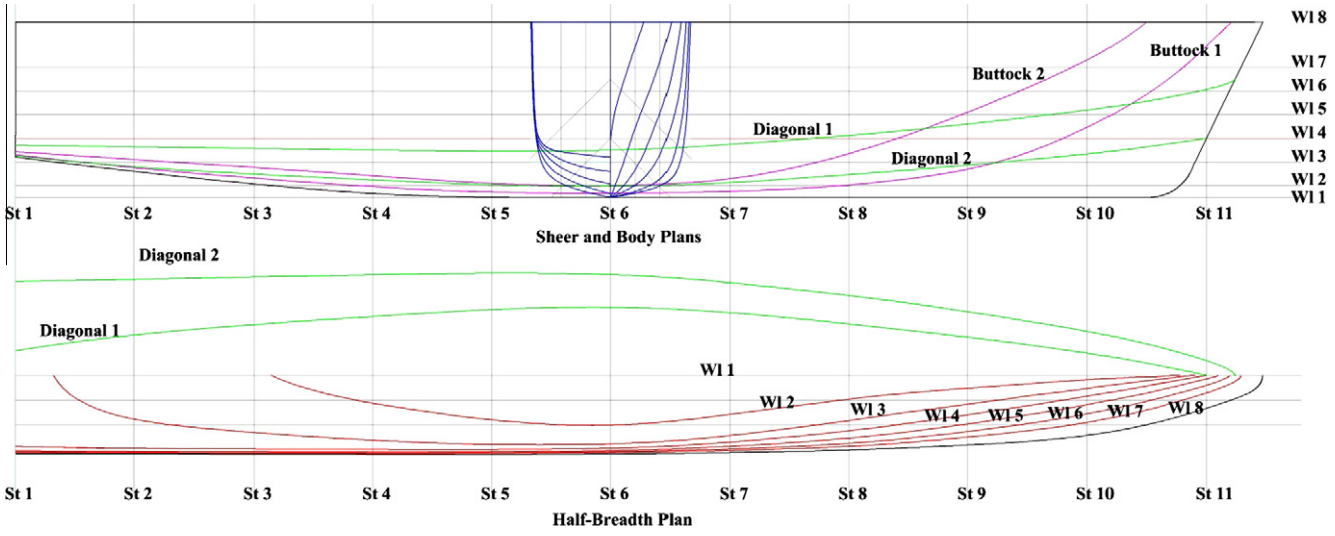

Figure 3 AMECRC©-09 parent model configuration.

nomenclature is used. L_W is the waterplane length of the parent model, B_W is the maximum waterplane breadth of the parent model, D_M is the maximum depth of the parent model, d_M is the maximum draft of the parent model, C_B is the block coefficient of the parent model, C_P is the prismatic coefficient of the parent model, C_M is the maximum section area coeffi-

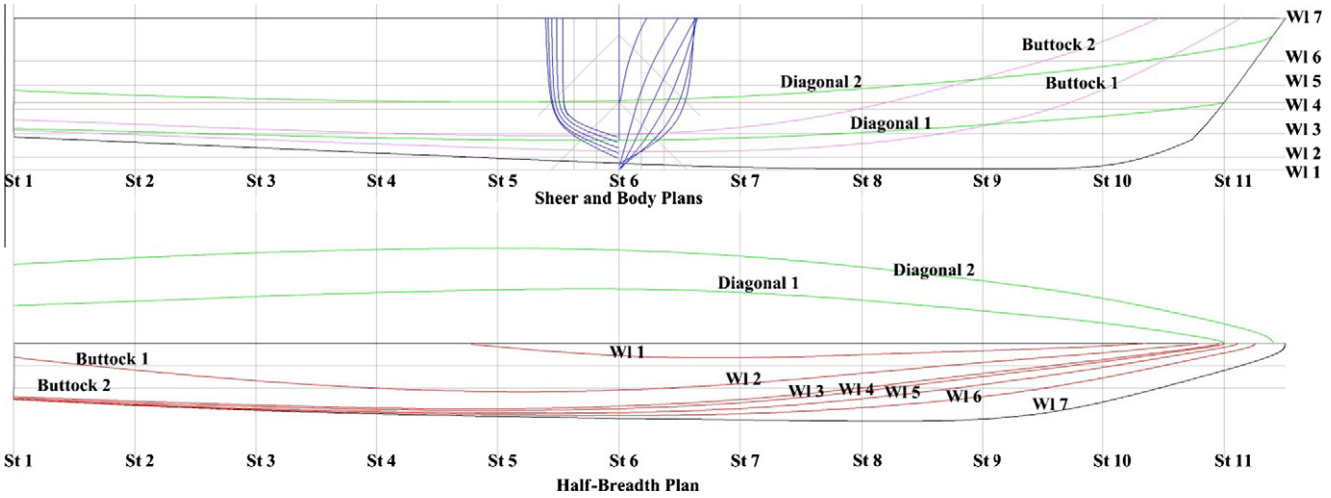

Figure 4 NPL©-4a parent model configuration.

Table 1 Principal particulars of Wigley©-st, AMECRC©-09 and NPL©-4a parent models.

Design parameter	Wigley©-st		AMECRC©-09		NPL©-4a	
	Main hull	Side hull	Main hull	Side hull	Main hull	Side hull
L_W (m)	50.0000	25.0000	50.0000	25.0000	50.0000	25.0000
B_W (m)	5.0000	2.5000	6.2530	3.1265	5.5730	2.7865
D_M (m)	6.2500	3.1250	7.4000	3.7000	6.2610	3.1305
d_M (m)	3.1250	1.5625	2.5000	1.2500	2.7850	1.3925
C_B	0.4440		0.4990		0.3940	
C_P	0.6670		0.6210		0.6840	
C_M	0.6670		0.8110		0.6550	
C_W	0.6670		0.7930		0.7600	
Δ (tonnes)	355.9000	44.4876	400.2000	50.0248	313.6000	39.2000
A_S (m^2)	371.9660	92.9915	365.8430	91.4608	330.3620	82.5905
A_M (m^2)	10.4160	2.6040	12.5650	3.1413	8.9400	2.2350
A_W (m^2)	166.6620	41.6655	248.0010	62.0002	211.8380	52.9595
LCB (%L_W)	50.0000 (ford Aft Perp.)		44.5620 (ford Aft Perp.)		43.6840 (ford Aft Perp.)	
LCF (%L_W)	50.0000 (ford Aft Perp.)		41.1550 (ford Aft Perp.)		41.7320 (ford Aft Perp.)	
KB (m)	1.9530	0.9765	1.5730	0.7865	1.9250	0.9625
BM_T (m)	0.6860	0.3430	1.7380	0.8690	1.3890	0.6945
BM_L (m)	60.0030	30.0015	97.2330	48.6165	103.5550	51.7775
TPC (tonnes/cm)	1.7080	0.4270	2.5420	0.6355	2.1710	0.54275
MCT1.0 cm (tonnes m)	4.4100	0.5513	7.9080	0.9885	6.6150	0.8269
$L_W/V^{1/3}$	7.1138		6.8410		7.4203	
L_W/B_W	10.0000		7.9962		8.9718	
B_W/d_M	1.6000		2.5012		2.0011	
λ	1.0000	0.5000	1.0000	0.5000	1.0000	0.5000

cient of the parent model, C_W is the waterplane area coefficient of the parent model, Δ is the displacement of the parent model, A_s is the witted surface area of the parent model, A_M is the maximum transverse section area of the parent model, A_W is the waterplane area of the parent model, LCB is the longitudinal center of buoyancy of the parent model expressed as percentage of its waterplane length, LCF is the longitudinal center of floatation of the parent model expressed as percentage of its waterplane length, KB is the vertical center of buoyancy of the parent model, BM_T is the transverse metacentric radius of the parent model, BM_L is the longitudinal metacentric radius of the parent model, TPC is the tonne per centimeter immersion of the parent model, MCT1.0 cm is the moment causing trim 1.0 cm of the parent model, $L_W/V^{1/3}$ is the slenderness ratio of the parent model, L_W/B_W is the waterplane length-to-maximum breadth ratio of the parent model, B_W/d_M is the waterplane maximum breadth-to-draft ratio of the parent model, λ is the trimaran main-to-side hulls scale factor.

The idea behind which Wigley©-st, AMECRC©-09, and NPL©-4a models are used in the present research is not only due to the availability of the numerical and experimental data describing the flow around them, but also due to few important hydrodynamic reasons.

Concerning Wigley©-st model, as it has a parabolic form ($\theta_E = 10.5°$), it may be modeled exactly in Maxsurf©, and therefore any deviation in its geometrical configuration, or in

its numerical results may be well recognized and interpreted. θ_E is the half angle of entrance of the parent model. Also, Wigley©-st model has a thin and sharp bottom ($\theta_D = 38.5°$), bow, and stern with the result of its insensitivity to the pressure fields at such regions. θ_D is the dead-rise angle at 50% L_W of the parent model. In addition, Wigley©-st is a non-transom model, and therefore the hydrodynamic problems associating the transom-stern; i.e., the vague vertices formation at higher F_n, the flow unsteadiness, and the apparent spray pattern (rooster tail) on the free surface behind the model do not exist.

Concerning AMECRC©-09 model, it is designed for operation at $0.10 \leqslant F_n \leqslant 1.0$, and LCB positioned in the aft body. The hull form is characterized by fairly rounded entrance waterline ($\theta_E = 13°$), almost V-type bow sections except a shallow flare at the far ford section, rounded aft body sections, straight buttock lines terminating smoothly at the transom, and shallower dead-rise ($\theta_D = 13°$).

Concerning NPL©-4a model, it is designed for operation at $0.30 \leqslant F_n \leqslant 1.20$, and LCB positioned in the aft body. The hull form is characterized by straight entrance waterlines ($\theta_E = 11°$), apparent flared bow sections near the design waterline, rounded aft body sections, straight buttock lines terminating sharply at the transom, and significant bottom dead-rise($\theta_D = 32.5°$).

3. Coordinate system and notations

In Maxsurf© [2] package and its downstream analysis modules, a right-handed trimaran-fixed coordinate system is used. The positive directions of such coordinate system are arbitrarily selected to be forward for the longitudinal axis x, starboard side for the transverse axis y, and up for the vertical axis z, with their origin arbitrarily positioned at the intersection of the aft perpendicular with the central longitudinal plane of the main hull. Fig. 5 shows the schematic view of the coordinate system and dimensional notation of the analysis trimaran. The percentages of stagger α and separation β with respect to L_W and B_W respectively are given in Eqs. (1) and (2).

$$\alpha = x/L_W \cdot 100 \tag{1}$$

$$\beta = y/B_W \cdot 100 \tag{2}$$

4. Resistance calculations

Hullspeed© [1] as a module of Maxsurf© [2] package is essentially a resistance calculation program, which uses SBM in addition to a number of regression-based methods. SBM embedded in Hullspeed© [1] is based on the work of Tuck et al. [30] and Couser et al. [31]. Basically, it calculates the ship energy dissipated in generating the free surface wave pattern, and hence the ship's wave-making resistance. SBM may be applied to many different hull form configurations including multihulls, but the individual hulls should be slender and symmetric about their central planes. In applying SBM, hulls with transom sterns are dealt with by automatically adding a virtual appendage, which is not the case with the non-transom stern hulls. Figs. 6–8 show the slender body mesh for Wigley©-st, AMECRC©-09, and NPL©-4a symmetric trimarans at $\alpha = +5\%$ and $\beta = +200\%$. The influence of both parallel sinkage and trim of the trimaran models, as well as the planning forces which limit the speed range applicability of SBM are not considered in this investigation.

Hullspeed© [1] breaks down the calm water total resistance of a trimaran $R_{t_{tri}}$ into the two conventional components which scale according to different resistance laws; Froude number dependent component, i.e. wave resistance $R_{w_{tri}}$ or residuary resistance $R_{r_{tri}}$ and a Reynolds number dependent component, i.e. viscous resistance $R_{v_{tri}}$ or friction resistance $R_{f_{tri}}$.

In terms of coefficients, and neglecting the wave-breaking, eddy and appendage resistances, the calm water total resistance of a trimaran may be expressed as given in Eqs. (3) or (4)

$$C_{t_{tri}} = C_{w_{tri}} + C_{v_{tri}} + C_{a_{tri}} \tag{3}$$

$$C_{t_{tri}} = C_{r_{tri}} + C_{f_{tri}} + C_{a_{tri}} \tag{4}$$

where $C_{t_{tri}}, C_{w_{cnt}}, C_{v_{tri}}, C_{r_{tri}}$, and $C_{f_{tri}}$ are the total, wave-making, viscous, residuary, and frictional resistance coefficients of the trimaran respectively. $C_{a_{tri}}$ is a correlation allowance of the trimaran, encompassing roughness allowance, particularities of the measuring device of the model basin, errors in the model-ship correlation line and the method. $C_{t_{tri}} = 0.0004$ is adopted throughout the present numerical calculations [32].

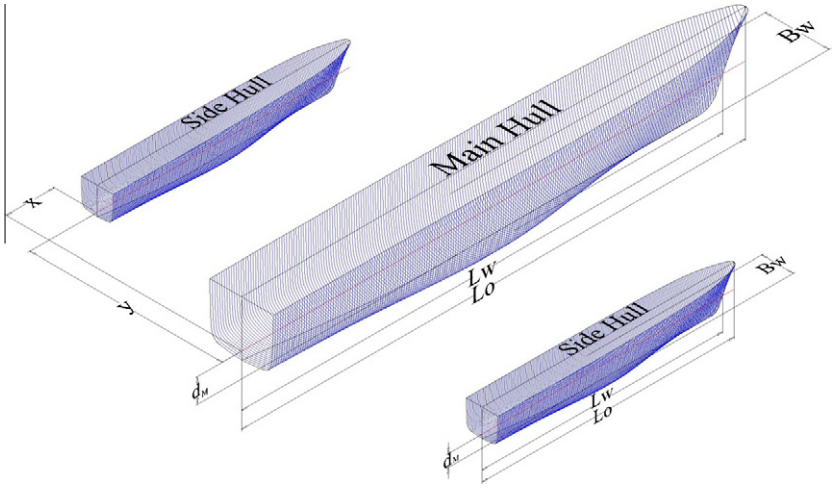

Figure 5 Schematic view of the coordinate system and dimensional notation of the analysis trimaran.

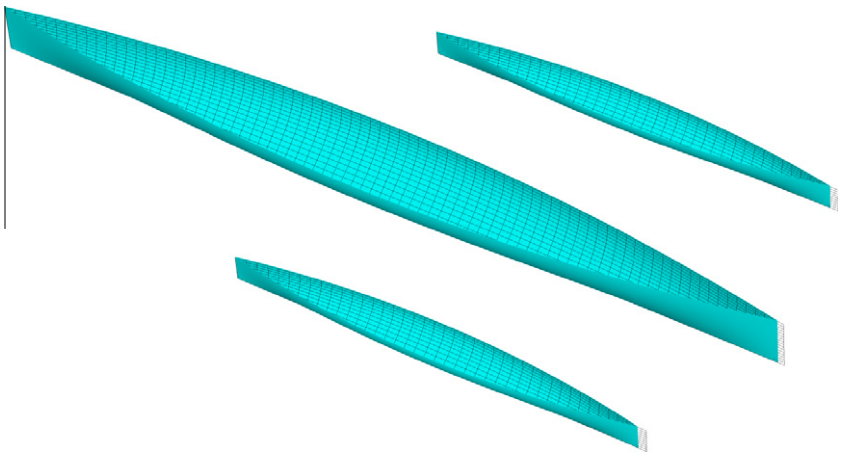

Figure 6 Slender body mesh of Wigley©-st symmetric trimaran at $\alpha = +5\%$ and $\beta = 200\%$.

Figure 7 Slender body mesh of AMECRC©-09 symmetric trimaran at $\alpha = +5\%$ and $\beta = 200\%$.

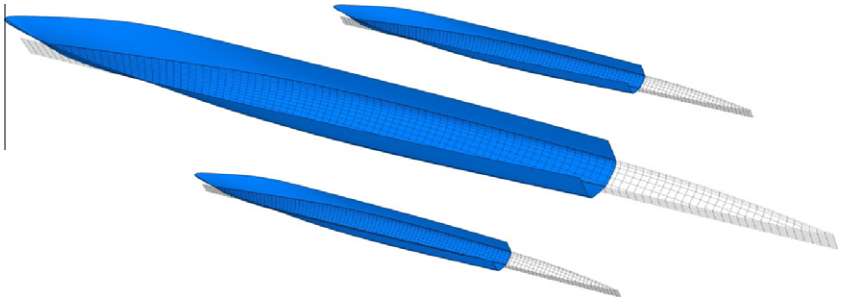

Figure 8 Slender body mesh of NPL©-4a symmetric trimaran at $\alpha = +5\%$ and $\beta = 200\%$.

In terms of the standard notation, the individual components of the trimaran calm water resistance coefficients may be represented as given in Eqs. (5)–(8) respectively.

$$C_{w_{tri}} = R_{w_{tri}}/0.5\rho A_{S_{tri}} U^2 \tag{5}$$

$$C_{v_{tri}} = R_{v_{tri}}/0.5\rho A_{S_{tri}} U^2 \tag{6}$$

$$C_{r_{tri}} = R_{r_{tri}}/0.5\rho A_{S_{tri}} U^2 \tag{7}$$

$$C_{f_{tri}} = R_{f_{tri}}/0.5\rho A_{S_{tri}} U^2 \tag{8}$$

The calm water friction resistance coefficient of the non-interfered trimaran hulls $C_{f_{tri-NI}}$ may be calculated as given in Eq. (9).

$$C_{f_{tri-NI}} = (1/A_{S_{tri}}) \cdot [A_{S_{cnt}} C_{f_{cnt}} + 2A_{S_{out}} C_{f_{out}}] \tag{9}$$

where $C_{f_{cnt}}$ and $C_{f_{out}}$ are the calm water friction resistance coefficients of the main hull and one outrigger respectively, $A_{S_{tri}}, A_{S_{out}}$ and $A_{S_{tri}}$ are the wetted surface areas of the main hull, one outrigger and trimaran respectively and may be expressed as given in Eq. (10).

$$A_{S_{tri}} = A_{S_{cnt}} + 2A_{S_{out}} \tag{10}$$

The calm water frictional resistance coefficient of the main hull $C_{f_{cnt}}$ and of one outrigger $C_{f_{out}}$ may be calculated approximately using the ITTC'57 [32] turbulent correlation line as given in Eqs. (11) and (12) respectively.

$$C_{f_{cnt}} = 0.075/(\log_{10} R_{e_{cnt}} - 2)^2 \tag{11}$$

$$C_{f_{out}} = 0.075/(\log_{10} R_{e_{out}} - 2)^2 \tag{12}$$

The ITTC'57 salt water properties are salinity $\varepsilon = 3.5\%$, temperature $t = 15\ ^{\circ}\mathrm{C}$, density $\rho = 1025.90\ \mathrm{kg/m^3}$, and kinematic viscosity $v = 1.18831 \times 10^{-6}\ \mathrm{m^2/s}$.

The Reynolds numbers of the main hull $R_{e_{cnt}}$ and of one outrigger $R_{e_{out}}$ may be calculated as given in Eqs. (13) and (14) respectively.

$$R_{e_{cnt}} = UL_{W_{cnt}}/v \tag{13}$$

$$R_{e_{out}} = UL_{W_{out}}/v \tag{14}$$

where U is the trimaran velocity, and $L_{W_{cnt}}$ and $L_{W_{out}}$ are the waterplane length of the main hull and one outrigger respectively.

The calm water viscous resistance of the non-interfered trimaran hulls $C_{v_{tri-NI}}$ includes a form effect applied to the calm water friction resistance of the individual hulls, and may be calculated as given in Eqs. (15) and (16).

$$C_{v_{tri-NI}} = (1/A_{S_{tri}}) \cdot [A_{S_{cnt}} C_{v_{cnt}} + 2A_{S_{out}} C_{v_{out}}] \tag{15}$$

$$C_{v_{tri-NI}} = (1/A_{S_{tri}}) \cdot [A_{S_{cnt}} (1+k)_{cnt} C_{f_{cnt}} + 2A_{S_{out}} (1+k)_{out} C_{f_{out}}] \tag{16}$$

where $(1 + k)_{cnt}$ and $(1 + k)_{out}$ are the form factors of the main hull and one outrigger respectively, reflecting the 3D form effect of the main hull and one outrigger as well as the viscous interaction effects between the triple hulls constituting the trimaran. The form factors of the main hull and outrigger may be estimated using an empirical formula.

The calm water wave-making resistance coefficient of the non-interfered trimaran hulls $C_{w_{tri-NI}}$ may be calculated as given in the following equation:

$$C_{w_{tri-NI}} = (1/A_{S_{tri}}) \cdot [A_{S_{cnt}} C_{w_{cnt}} + 2A_{S_{out}} C_{w_{out}}] \tag{17}$$

where $C_{w_{cnt}}$ and $C_{w_{out}}$ are the calm water wave-making resistance coefficients of the main hull and one outrigger respectively.

The calm water residuary resistance coefficient of the non-interfered trimaran hulls $C_{r_{tri-NI}}$ may be calculated as given in Eq. (18).

$$C_{r_{tri-NI}} = C_{w_{tri-NI}} + (1/A_{S_{tri}}) \cdot [A_{S_{cnt}} k_{cnt} C_{f_{cnt}} + 2A_{S_{out}} k_{out} C_{f_{out}}] \tag{18}$$

Combining Eqs. (9) and (17), then the sum of the calm water total resistance coefficients of the non-interfered trimaran hulls $C_{r_{tri-NI}}$ may be calculated as given in Eq. (19).

$$C_{t_{tri-NI}} = (1/A_{S_{tri}}) \cdot [A_{S_{cnt}} C_{t_{cnt}} + 2A_{S_{out}} C_{t_{out}}] \tag{19}$$

where $C_{t_{cnt}}$ and $C_{t_{out}}$ are the calm water total resistance coefficients of the main hull and one outrigger respectively.

5. Interference factor η

The calm water resistance of the trimaran bonded-hulls drastically varies from that of the non-bonded hulls. To evaluate the hydrodynamic interference effects of each individual design configurations, the interference factor η may be calculated as the difference in total resistance captured when moving from separate triple hulls into one bonded trimaran. It is convenient to express such difference as a ratio of the non-interfered total resistance as given in Eq. (20).

$$\eta = C_{t_{tri}}/C_{t_{tri-NI}} - 1.0 \tag{20}$$

A negative interference factor indicates a beneficial interference; i.e., the resistance of the trimaran configuration is less than the aggregate resistances of the individual hulls; whereas a positive interference factor implies an existence of a detrimental interference.

6. Automation and programming implementation

Maxsurf© [2] CAD package and its downstream analysis modules provide direct automation support that allows the interested user to create, modify and analyze many design models over a minimum time span. None of the Maxsurf© [2] modules include an embedded environment to write or record macros, but they accept their interface via the conventional programming languages, e.g., Visual C^{++}©, Visual Basic©, Visual FORTRAN©, Java©, or Microsoft© Windows© Scripting Host©, etc. Also, all Maxsurf© [2] modules have the ability to interface spreadsheet applications like Microsoft© Office©, other CAD systems like Autodesk© AutoCAD©, and other graphing systems like SigmaPlot©, to either get more design details or to get more visualization quality.

Seeking automation of the rigorous resistance calculation procedures of the three trimaran series, a sophisticated computer macro-named Tri-PL© is developed from scratch based on the Visual Basic for Applications© [8]. To generate each model of the three individual trimaran series together with its detailed hydrostatic particulars, Tri-PL© automatically interferes Maxsurf© [2] module. To calculate the calm water resistance components for each model of the three individual trimaran series, Tri-PL© automatically interferes Hullspeed© [1] module. To visualize the significant analysis data of Tri-PL© properly, a graph template of SigmaPlot© [9] is created. Fig. 9 depicts the scheme of the resistance calculation procedures of Wigley©-st, AMECRC©-09, and NPL©-4a trimaran series.

The time necessary for generating each of the three individual trimaran series of Wigley©-st, AMECRC©-09, and NPL©-4a together with the detailed calculation of the hydrostatic particulars, resistance and data visualization is almost about 21000*CPU* seconds on an Intel© *i*5 2.40 GHz, 3*MB cash*, and 4 GB *DDR*3 Dell© Inspiron-1545 Labtop.

7. Validation and benchmarking

Both Wigley©-st and AMECRC©-09 models are selected to validate the accuracy and homogeneity of SBM numerical results, as well as benchmarking the newly developed computer macro-Tri-PL©. For the validation purposes only, the scale ratio of the side-to-main hulls of Wigley©-st and AMECRC©-09 models $\lambda = 0.500$ and $\lambda = 0.459$ respectively.

Fig. 10 shows the variation of $C_{w_{tri}}$ versus F_n for one Wigley©-st symmetric trimaran model corresponding to $\alpha = 0\%$ and $\beta = 131.24\%$, calculated by both Michlet© [33] computer program and Hullspeed© [1] via Tri-PL© macro. In such validation, the numerical results of Hullspeed© [1] via Tri-PL© macro-seem to agree very well with those of Michlet© [33], and both confirm the validation of Hullspeed© [1].

Fig. 11 shows the variation of $C_{w_{tri}}$ versus F_n for three AMECRC©-09 symmetric trimaran models corresponding to

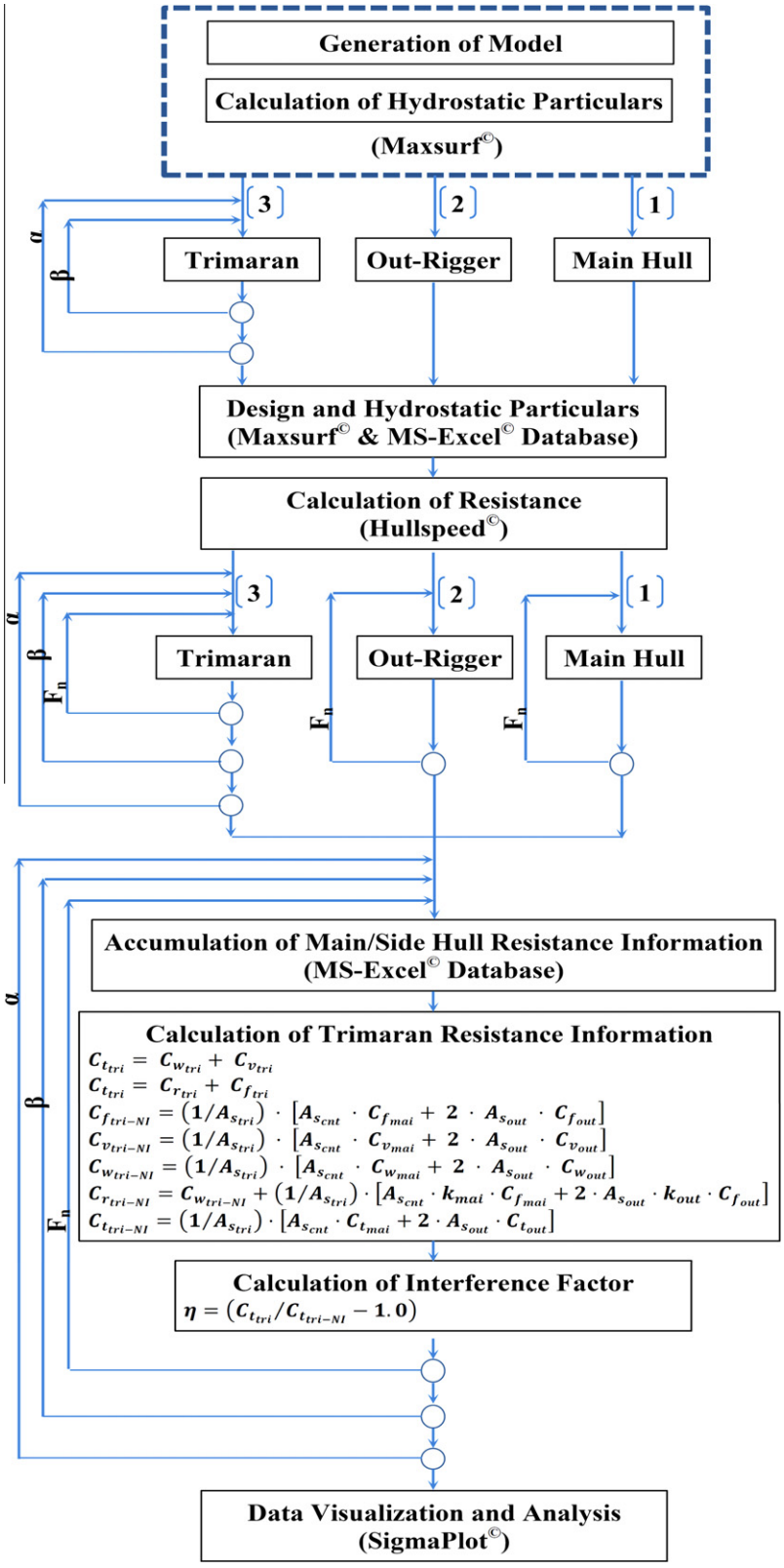

Figure 9 Scheme of the resistance calculation procedures of the analysis trimaran.

$\alpha = -20\%$, -30% and -40% all at $\beta = 160\%$, predicted by four methods. The latter methods include 2D SBM, experiments, and 3D potential flow panel method of ShipFlow©, already published by Mynard et.al. [34] as well as the numerical results of the Hullspeed© [1] via Tri-PL© macro. In such validation, the numerical results of Hullspeed© [1] via

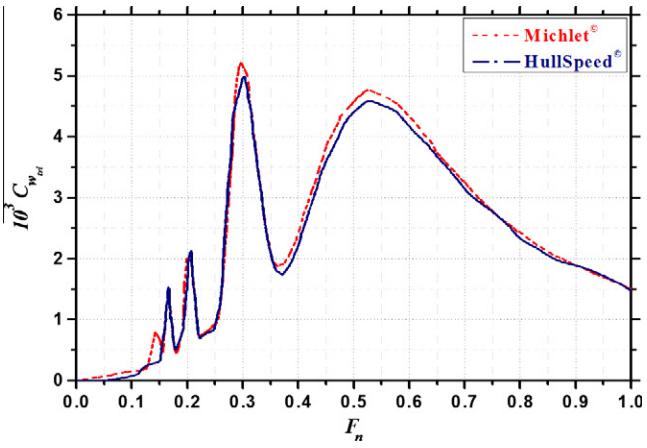

Figure 10 Validation of $C_{w_{tri}}$ versus F_n for the Wigley©-st symmetric trimaran at $\alpha = 0.0\%$ and $\beta = 131.60\%$.

Tri-PL© macro-seem to agree very well with the numerical results of [34] along the considered F_n interval $0.20 \leqslant F_n \leqslant 1.0$. The results highlight a substantial increase in $C_{w_{tri}}$ toward decreasing α for the same β, showing the influence of the hydrodynamic interference beneath the triple hulls. The situation is different with the ShipFlow©; where the trend of its results seem to agree with that of the Hullspeed© [1] via Tri-PL© macro-over the interval $0.45 \leqslant F_n \leqslant 1.0$, but over-predicting $C_{w_{tri}}$ along the interval $0.30 \leqslant F_n \leqslant 0.45$. The numerical results of Hullspeed© [1] via Tri-PL© macro-records a seemingly mismatched $C_{w_{tri}}$ results in the different F_n zones with the experimental results of [34]; matching the other two numerical results in recording a clear under-prediction of $C_{w_{tri}}$.

Palpably, the aforementioned numerical results differ from each other and from the experimental one due to the ways considered therein in manipulating the transom stern, the bow wave-breaking resistance, the viscous drag, the eddy formation, the forward thrust of the viscous pressure fields, the flow separation around the hull, the mutual interaction beneath the resistance components, and the rooster tail behind the model. Also, the reliability of the experimental results is principally based on the ship-model scaling, accuracy of the recording gauges, and the technicians' capabilities.

8. Analysis of the numerical results

Figs. 12a–12d shows the 3D envelop variation of η versus F_n and β for Wigley©-st, AMECRC©-09, and NPL©-4a symmetric trimaran series respectively at twelve arbitrarily selected staggers, $\alpha = -50\%$, -35%, -20%, -05%, 0%, $+10\%$, $+25\%$, $+25\%$, $+40\%$, $+55\%$, $+70\%$, $+85\%$, and $+100\%$. For comparative depiction of the three developed trimaran series, each row represents the envelop of η for Wigley©-st, AMECRC©-09, and NPL©-4a trimarans at the specified α. For convenient interpretation of the graphs, the appropriate trimaran configuration at the arbitrarily selected α and $\beta = 150\%$ appears on the relevant envelope.

A hollow represents a negative interference which is beneficial; i.e., the resistance of the corresponding trimaran configuration is less than the non-interfered resistances; whereas a hump signifies a positive interference which is detrimental. A flat envelop indicates a zero interference which is idle (non-beneficial); i.e., the resistance of the corresponding trimaran configuration equals the non-interfered resistances. The interference effects may be reverted to the constructive/destructive interaction of the individually induced bi-wave systems, the wave-induced variations in the tri-wetted surface areas, and/or the induced mutual pressure gradients. Such interference effects almost vanish at higher separations, on the penalty of difficult docking and stiff transverse stability.

The pressure carrying the trimaran may be divided into hydrostatic and hydrodynamic. The hydrostatic pressure gives the buoyancy force, which is proportional to the submerged displacement volume of the trimaran; whereas, the hydrodynamic pressure depends on the flow around the hull and is approximately proportional to the ship speed squared. For $F_n \leqslant 0.45$, the buoyancy force dominates relative to the hydrodynamic force, and the trimaran is termed displacement. For $0.45 \leqslant F_n \leqslant 1.0$, the hydrodynamic force dominates relative to the buoyancy force and the trimaran is termed semi-displacement. Generally, frictional resistance dominates at lower speeds, whereas, the wave-making resistance dominates as the speed increases. However, for a slender fine trimaran, as its wetted surface area increases, its frictional resistance increases too, and its wave-making resistance reduces at higher speeds.

Starting at $\alpha = -50\%$, few hollows of η appear at scattered F_n intervals and extending over unequal wide intervals of β; such hollows appear to assume specific backward skewed trends which differs from a series configuration to another and from F_n interval to another for the same model configuration in a series.

A maximum hollow $\eta = -0.30$ appears in the transition zone extending over the intervals $0.47 \leqslant F_n \leqslant 0.49$ and $265\% \leqslant \beta \leqslant 275\%$ (Wigley©-st), $0.435 \leqslant F_n \leqslant 0.585$ and $100\% \leqslant \beta \leqslant 305\%$ (AMECRC©-09), as well as $0.47 \leqslant F_n \leqslant 0.52$ and $215\% \leqslant \beta \leqslant 300\%$ (NPL©-4a). Also, for (NPL©-4a), another hollow $\eta = -0.20$ appears in the displacement zone extending over the intervals $0.31 \leqslant F_n \leqslant 0.34$ and $100\% \leqslant \beta \leqslant 175\%$. Zones of $\eta = 0.0$ appear scattered in a portion of the displacement zone $F_n \leqslant 0.45$ (Wigley©-st), $F_n \leqslant 0.45$ (AMECRC©-09), and $F_n \leqslant 0.30$(NPL©-4a). Zones of $\eta = 0.0$ extends over a significant circular area in the semi-displacement zone intersecting $\beta = 100\%$ at $F_n = 0.94$ and $\beta = 400\%$ at $F_n = 0.56$ (Wigley©-st), intersecting $\beta = 100\%$ at $F_n = 0.845$ and $\beta = 400\%$ at $F_n = 0.535$ penetrated with a hump $\eta = 0.1$ (AMECRC©-09), and intersecting $\beta = 100\%$ at $F_n = 0.91$ and $\beta = 400\%$ at $F_n = 0.56$(NPL©-4a). Arbitrary humps of η appear scattered in the displacement zone $F_n \leqslant 0.40$ covering the whole separation interval $100\% \leqslant \beta \leqslant 400\%$, with the worst hump, $\eta = +0.40$ appears to concentrate around $F_n = 0.29$ and $\beta = 100\%$ (Wigley©-st), $\eta = +0.30$ appears to concentrate around $F_n = 0.37$ and $\beta = 100\%$ (AMECRC©-09), and $\eta = +0.20$ appears to concentrate around $F_n = 0.375$ and $\beta = 250\%$ (NPL©-4a).

As α increases by moving the outriggers forward closer to the central main hull, the hollows of η move toward the lower F_n region, extending over limited separation intervals, and diminishes rapidly toward $\alpha = +130\%$ (Wigley©-st), $\alpha = +14\%$ (AMECRC©-09), and $\alpha = -5.0\%$ (NPL©-4a).

At $\alpha = +14\%$, except a single backward skewed hump $\eta = +0.30$ at $\beta = 100\%$ and $F_n = 0.45$, and a few scattered skewed hollows $\eta = -0.10$ in a portion of the displacement zone $F_n \leqslant 0.33$ (Wigley©-st), and a single backward skewed hump $\eta = +0.30$ at $\beta = 100\%$ and $F_n = 0.47$ (AMECRC©-

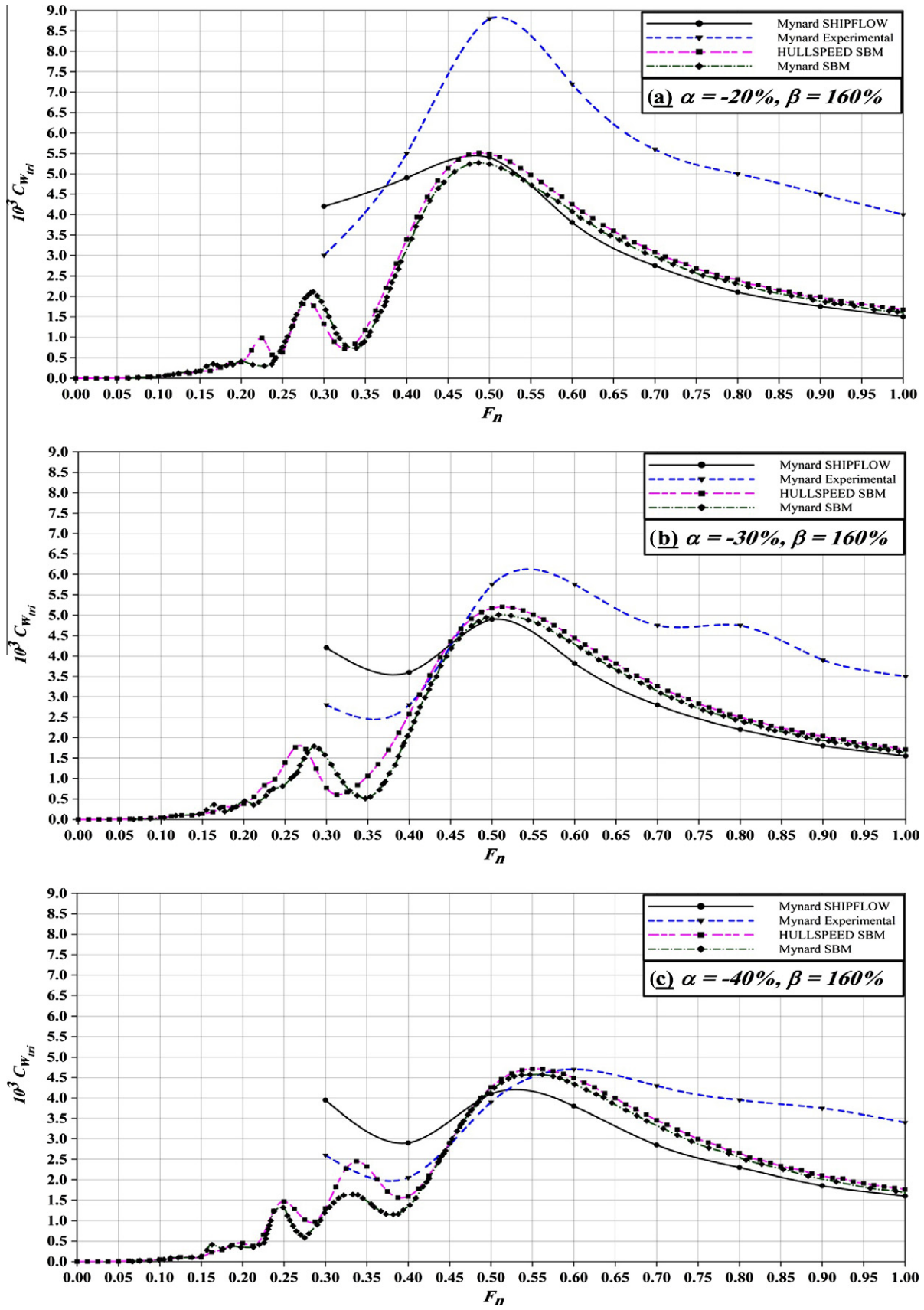

Figure 11 Validation of $C_{W_{tri}}$ versus F_n for AMECRC©-09 symmetric trimaran for (a) $\alpha = -20.0\%$, $\beta = 160\%$, (b) $\alpha = -30.0\%$, $\beta = 160\%$, and (c) $\alpha = -40.0\%$, $\beta = 160\%$.

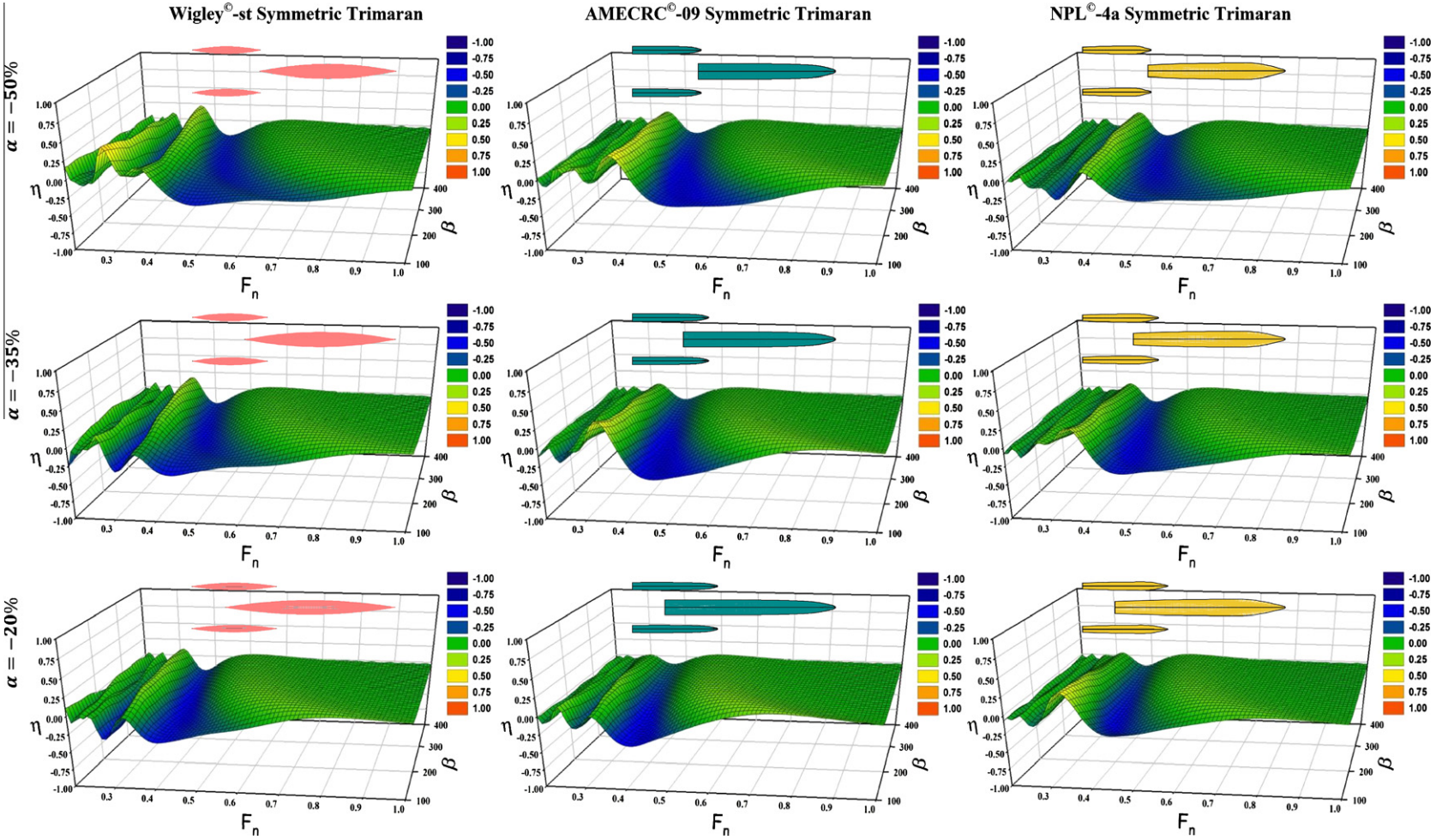

Figure 12a Variation of η versus F_n and β for Wigley©-st, AMECRC©-09, and NPL©-4a symmetric trimaran series at $\alpha = -50\%$, -35%, and -20%.

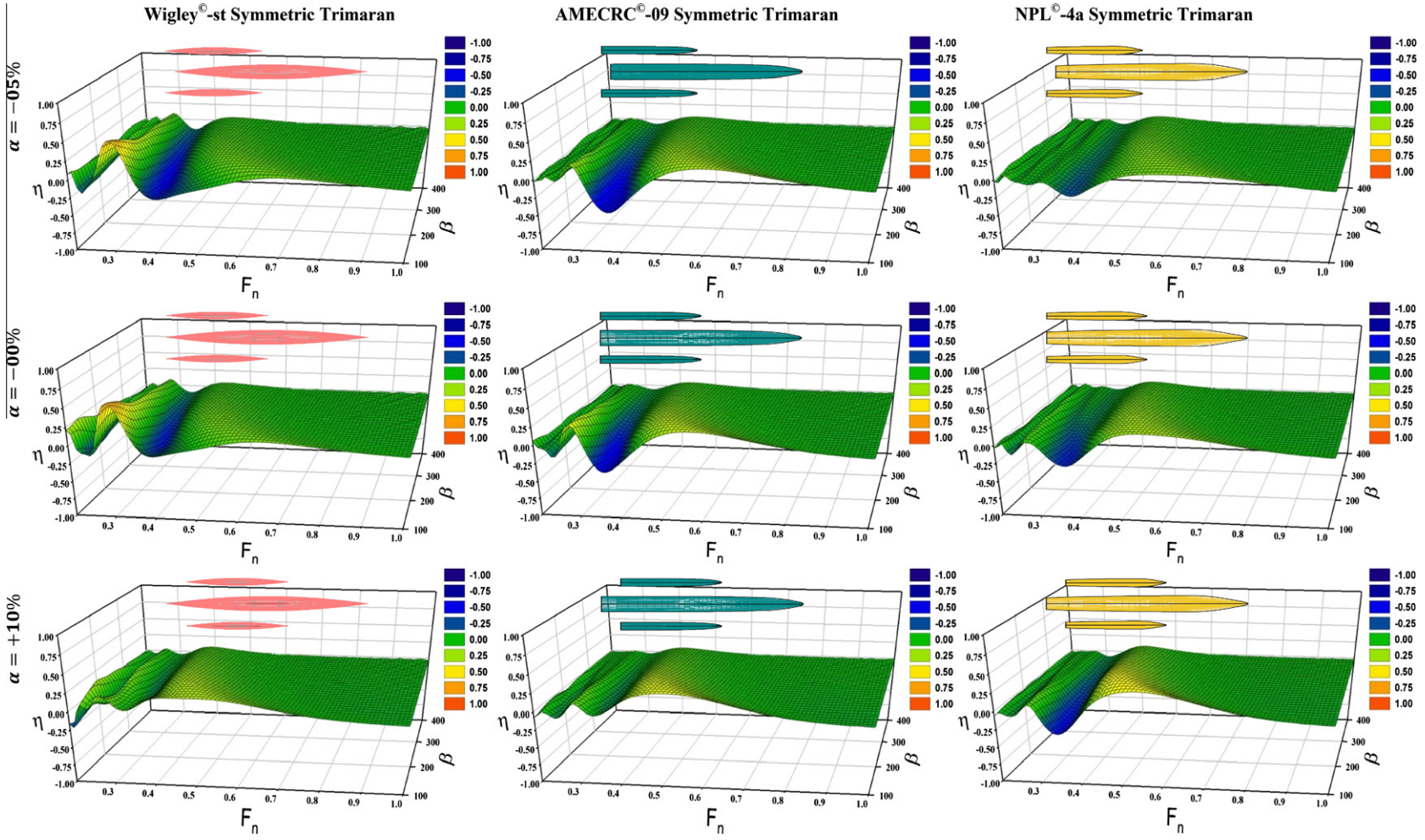

Figure 12b Variation of η versus F_n and β for Wigley©-st, AMECRC©-09, and NPL©-4a symmetric trimaran series at $\alpha = -5.0\%$, 0.0%, and 10%.

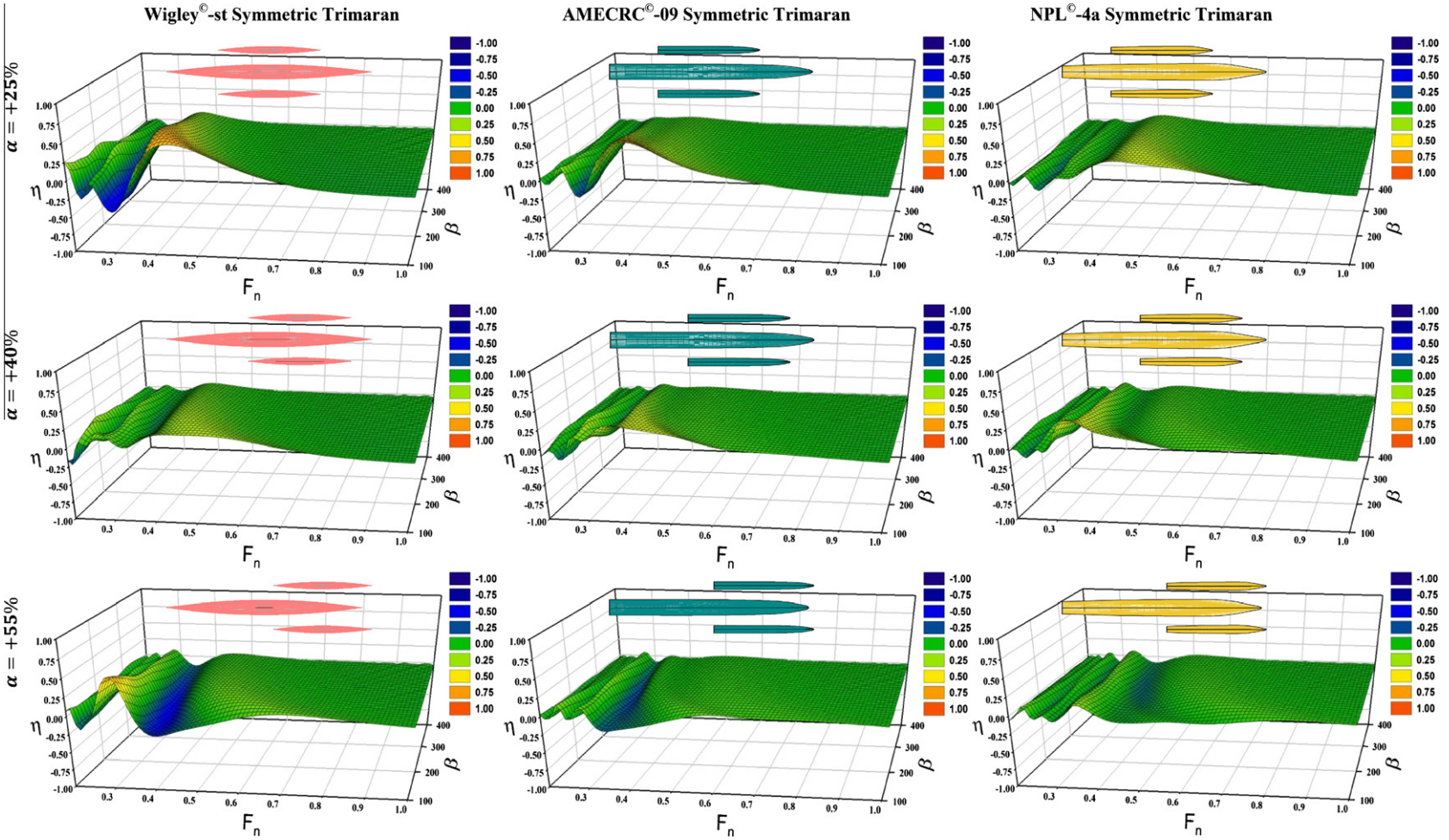

Figure 12c Variation of η versus F_n and β for Wigley©-st, AMECRC©-09, and NPL©-4a symmetric trimaran series at $\alpha = +25\%, +40\%$, and $+55\%$.

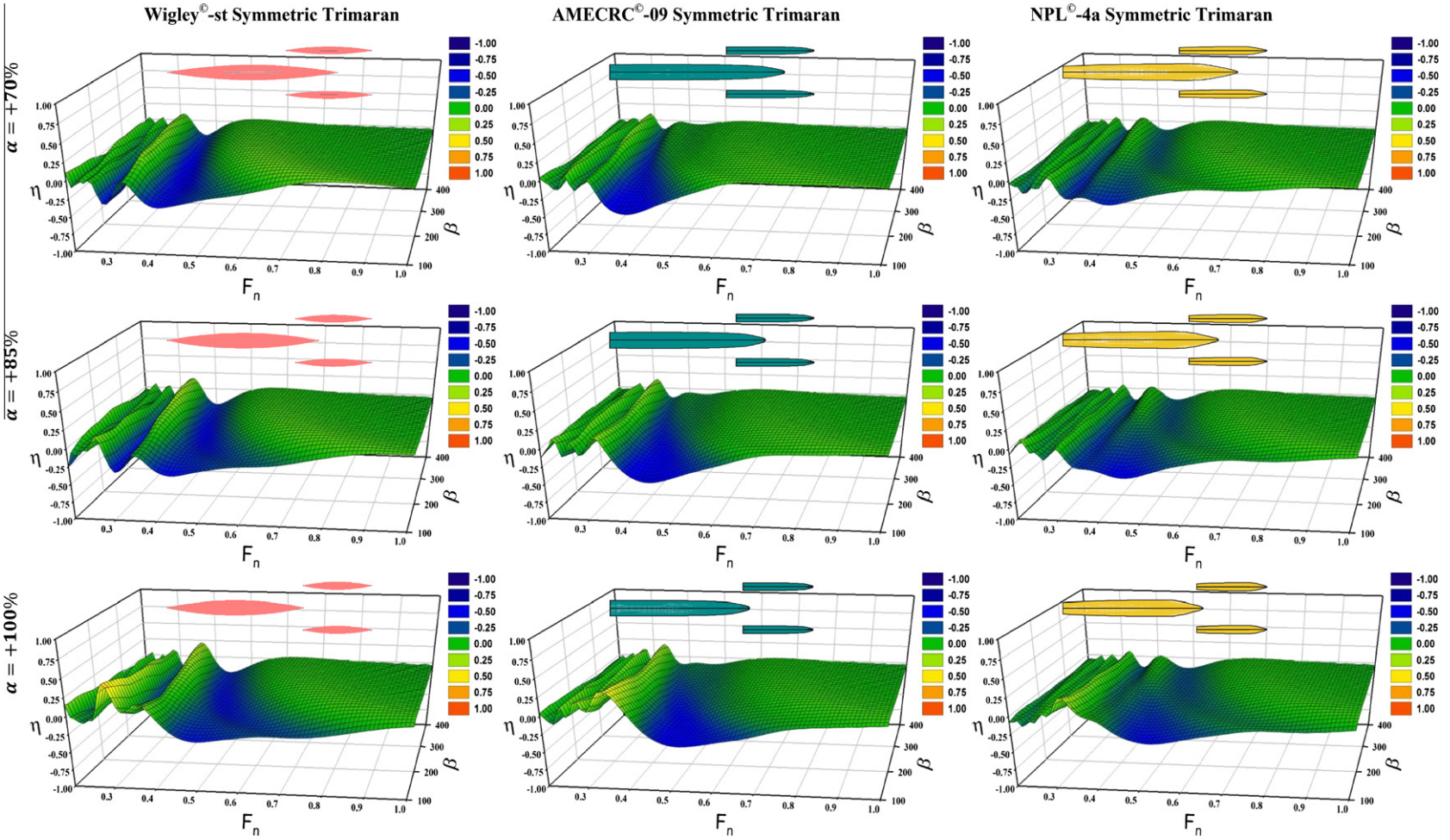

Figure 12d Variation of η versus F_n and β for Wigley©-st, AMECRC©-09, and NPL©-4a symmetric trimaran series at $\alpha = +70\%, +85\%$, and $+100\%$.

09), the variation of η with respect to β and F_n is a quite smooth flat surface $\eta = 0.0$ in both series, indicating that the interaction effects have progressively died-out.

For NPL©-4a, at $\alpha = -4.0\%$, except two backward skewed hollows $\eta = -0.20$ and $\eta = -0.10$ extend over $0.365 \leqslant F_n \leqslant 0.390$, $100\% \leqslant \beta \leqslant 175\%$ and $0.335 \leqslant F_n \leqslant 0.425$, $100\% \leqslant \beta \leqslant 325\%$ respectively, and a backward skewed hump $\eta = +0.10$ extends over $0.49 \leqslant F_n \leqslant 0.79$ and $100\% \leqslant \beta \leqslant 325\%$, the variation of η with respect to β and F_n is a quite smooth flat surface $\eta = 0.0$. As α increases further into the interval $-3.0\% \leqslant \alpha \leqslant +1.0\%$, two backward skewed hollows $\eta = -0.10$ and $\eta = -0.20$ developed over the intervals $0.225 \leqslant F_n \leqslant 0.240$, $100\% \leqslant \beta \leqslant 165\%$ and $0.30 \leqslant F_n \leqslant 0.40$, $100\% \leqslant \beta \leqslant 210\%$ respectively, in addition to a significant backward skewed hump $\eta = +0.20$ developed over the intervals $0.490 \leqslant F_n \leqslant 0.650$, $100\% \leqslant \beta \leqslant 210\%$. As α increases more further into the interval $+2.0\% \leqslant \alpha \leqslant +11.0\%$, a backward skewed hollow $\eta = -0.30$ developed over the intervals $0.30 \leqslant F_n \leqslant 0.40$, $100\% \leqslant \beta \leqslant 270\%$, beyond a significant backward skewed hump $\eta = +0.30$ developed over the intervals $0.490 \leqslant F_n \leqslant 0.600$, $100\% \leqslant \beta \leqslant 210\%$.

For Wigley©-st, as α increases further into the interval $+14\% \leqslant \alpha \leqslant +27\%$, two backward skewed humps $\eta = -0.30$ and $\eta = -0.20$ appear to concentrate around $F_n = 0.300$ and $F_n = 0.225$ respectively, in addition to a significant backward skewed hump $\eta = +0.50$ appears clearly in the interval $0.370 \leqslant F_n \leqslant 0.560$.

For AMECRC©-09, as α increases further into the interval $+15\% \leqslant \alpha \leqslant +18\%$, two backward skewed hollows $\eta = -0.10$ appear to concentrate around $F_n = 0.265$, $\beta = 105\%$ and $F_n = 0.275$, $\beta = 210\%$ respectively, in addition to a significant backward skewed hump $\eta = +0.40$ appears clearly at $F_n = 0.410$, and $\beta = 100\%$. As α increases more further into the interval $+19\% \leqslant \alpha \leqslant +26\%$, a backward skewed hollow $\eta = -0.20$ appears to concentrate around $F_n = 0.280$ and $\beta = 150\%$, beyond a significant backward skewed hump $\eta = +0.50$ appears clearly at $F_n = 0.400$ and $\beta = 100\%$.

For NPL©-4a, as α increases further into the interval $+12\% \leqslant \alpha \leqslant +31\%$, both the backward skewed hollow $\eta = -0.30$ and the backward skewed hump $\eta = +0.30$ moves gradually toward the lower F_n zone, and finally at $\alpha = +31\%$, except two double backward skewed humps $\eta = +0.20$ and $\eta = +0.10$ extend over $0.320 \leqslant F_n \leqslant 0.540$, $100\% \leqslant \beta \leqslant 145\%$ and $0.300 \leqslant F_n \leqslant 0.730$, $100\% \leqslant \beta \leqslant 335\%$ respectively, the variation of η with respect to β and F_n is a quite smooth flat surface $\eta = 0.0$. As α increases more further into the interval $+32\% \leqslant \alpha \leqslant +42\%$, triple hollows $\eta = -0.10$ developed arbitrarily over the intervals $0.200 \leqslant F_n \leqslant 0.300$, $100\% \leqslant \beta \leqslant 400\%$, in addition to a hump $\eta = +0.30$ developed over the intervals $0.320 \leqslant F_n \leqslant 0.385$, $100\% \leqslant \beta \leqslant 135\%$. As α increases more and more further into the interval $+43\% \leqslant \alpha \leqslant +50\%$, the triple hollows $\eta = -0.10$ and the hump $\eta = +0.30$ gradually vanish, with another three hollows $\eta = -0.10$, develop gradually over the intervals $0.250 \leqslant F_n \leqslant 0.255$, $180\% \leqslant \beta \leqslant 265\%$, $0.285 \leqslant F_n \leqslant 0.290$, $330\% \leqslant \beta \leqslant 375\%$, and $0.385 \leqslant F_n \leqslant 0.465$, $200\% \leqslant \beta \leqslant 375\%$ respectively.

Targeting the end of the outriggers track for both Wigley©-st, and AMECRC©-09, as α increases further into the interval $+27\% \leqslant \alpha \leqslant +100\%$, the pattern of humps and hollows seems to be regenerated reversely targeting a pattern similar to the starting pattern generated at $\alpha = -50\%$.

The fin situation is different for NPL©-4a; as α increases further into the interval $+51\% \leqslant \alpha \leqslant +100\%$, the pattern of humps and hollows regenerate targeting a pattern totally different from that at $\alpha = -50\%$. Arriving at $\alpha = +100\%$, a minute hollow $\eta = -0.10$ develop gradually over the intervals $0.225 \leqslant F_n \leqslant 0.235$, $100\% \leqslant \beta \leqslant 190\%$, in addition to horn-like backward skewed hollow $\eta = -0.10$ develop gradually intersecting $\beta = 100\%$ at $F_n = 0.420$ and $F_n = 0.740$, and $\beta = 400\%$ at $F_n = 0.345$, $F_n = 0.380$, $F_n = 0.450$ and $F_n = 0.540$. A significant backward skewed hollow $\eta = -0.30$ develop gradually intersecting $\beta = 100\%$ at $F_n = 0.500$ and $F_n = 0.560$ and extending over the interval $100\% \leqslant \beta \leqslant 130\%$. Three arbitrary scattered hollows $\eta = -0.10$ develop gradually in the intervals $0.200 \leqslant F_n \leqslant 0.300$, $100\% \leqslant \beta \leqslant 400\%$. Zones of $\eta = 0.0$ appear scattered in the displacement zone $F_n \leqslant 0.450$; whereas, it extends over a significant circular area in the semi-displacement zone intersecting $F_n = 1.000$ at $\beta = 110\%$ and $\beta = 400\%$ at $F_n = 0.630$.

9. Conclusions

This paper numerically investigates the influence of stagger variation of the outriggers on the hydrodynamic interference of three trimarans series. Unequivocally, brief investigations of the principal conclusions that may be aggregated from this research work are:

i. The computer macro-Tri-PL© surely represent a powerful design tool capable for integration into a sophisticated optimization technique to help the designer making his decision in the preliminary design stage; as alternative concepts have to be evaluated thoroughly and the principal dimensions must be selected in a rational way.
ii. Significant changes in some hull form parameters such as B_W/d_M results in insignificant changes in the amplitude and phase of η. Conversely, any minor changes in L_W/B_W ratio, results in pronounced changes in the amplitude and phase of η, which results principally from the associating changes in the amplitude and phase of the wave-making resistance.
iii. Above a shoulder speed, which is dependent on α, β, together with the immersed geometry of the considered trimaran model, η may be insignificant. This is an important feature for HST as it allows optimization of α and β for other design considerations, e.g., statical and/or dynamical stability, seakeeping without incurring significant penalties in calm water resistance.
iv. The trimaran performance measured hereby by the hydrodynamic interference η is more sensitive to the variation in α than in β. There is no unique trimaran configuration within any of the three generated series may generate beneficial interference over the entire or even a significant portion of the considered velocity interval $0.200 \leqslant F_n \leqslant 1.000$, as η fluctuates with velocity for each model.
v. For all β, the far aft and ford longitudinal positions, i.e., $\alpha = -50\%$ and $\alpha = +100\%$, perform well at low and high speed ranges, but perform poorly in the intermediate speed interval $0.240 \leqslant F_n \leqslant 0.340$. For all α, the most inboard separation, i.e., $\beta = 100\%$ performs well at

most of the speeds in the interval $F_n \leqslant 0.500$, but on the contrary side, it generates detrimental interference in the interval $F_n \geqslant 0.500$.

vi. Practically, creating beneficial interferences, or at least minimizing detrimental ones, represent vital issues that should be addressed in designing a reliable trimaran configuration.

Recommendations

Clear recommendations that may serve as guidelines for a futuristic sophisticated prediction of the hydrodynamic interference of HST are:

i. The influence of parallel sinkage, trim, and main-to-side hulls draft variation on the prediction of the hydrodynamic interference of HST should be considered in a future research work.
ii. A computational fluid dynamics (CFDs) program should be used to simulate the flow past the aforementioned three trimaran series, Wigley©-st, AMECRC©-09, and NPL©-4a, in order to calculate more accurately the hydrodynamic interference, and then validate the outcomes of this research against.
iii. A comprehensive experimental work needs to be undertaken to validate both the numerical calculations and simulations, and then propose a regression model for rapid resistance estimation of the trimaran.

Acknowledgments

The corresponding author would like to express his grateful thanks to both Maxsurf© team, Formation Design Systems, Australia, and SigmaPlot© team, Systat Software Inc., UK; for their sincere help and support. The views, opinions, and conclusions expressed herein are those of the corresponding author, for which he is alone should be held responsible.

References

[1] Hullspeed©, Formation Design Systems Pty. Ltd., 2011.
[2] Maxsurf©, Formation Design Systems Pty. Ltd., 2011.
[3] W. Wigley, A comparison of experimental and calculated wave profiles and wave resistances for a form having parabolic waterlines, Proc. Roy. Soc. London, Ser. A 144 (851) (1934) 144–159.
[4] P. Bojovic, AMECRC Systematic Series Calm Water Testing Results, Australian Maritime Engineering Cooperative Research Centre, Report AMECRC IR 95/5, 1995, pp. 1–93.
[5] P. Bojovic, G. Goetz, Geometry of AMECRC Systematic Series, Australian Maritime Engineering Cooperative Research Centre, Report AMECRC IR 96/6, 1996, pp. 1–37.
[6] W. Marwood, D. Bailey, Design Data for High-speed Displacement Hulls of Round-bilge Form, Ship Report 99, National Physical Laboratory, 1969.
[7] D. Bailey, The NPL High Speed Round Bilge Displacement Hull Series, Marine Technology Monograph, The Royal Institute of Naval Architects (RINA), vol. 4, 1976.
[8] Visual Basic for Applications©, Microsoft© Corp., 2010.
[9] SigmaPlot©, Systat Software Inc., 2006.
[10] K. Kang, S. Kim, Y. Choi, Seakeeping and maneuvering performances of the 2500 tons class trimaran, in: Proc. 2nd Int. Workshop on Ship Hydrodynamics (IWSH'01), China, 2001, pp. 38–44.
[11] J. Wilson, Sea Power 2000, Popular Mechanics, 1999.
[12] H. Xu, Z. Zou, Numerical prediction of wave-making resistance of a trimaran, in: Proc. 2nd Int. Workshop on Ship Hydrodynamics (IWSH'01), China, 2001, pp. 105–109.
[13] J. Michell, The wave resistance of a ship, Philos. Mag., Engl. 5 (45) (1898) 106–123.
[14] M. Insel, A. Molland, An investigation into the resistance components of high speed displacement catamarans, Trans. Roy. Inst. Naval Architects (RINA) 11 (9) (1991).
[15] L. Doctors, M. Renilson, G. Parker, N. Hornsby, Waves and wave resistance of a high-speed river catamaran, in: Proc. 1st Int. Conference on Fast Sea Transportation (FAST'91), Norwegian Institute of Technology, Norway, vol. 1, 1991, pp. 35–52.
[16] L. Doctors, M. Renilson, Corrections for finite-water-depth effects on ship resistance, in: Proc. 11th Australasian Fluid Mechanics Conference (AFMC'92), University of Tasmania, Tasmania, vol. 1, 1992, pp. 663–666.
[17] L. Doctors, M. Renilson, The influence of demi-hull separation and river banks on the resistance of a catamaran, in: Proc. 2nd Int. Conference on Fast Sea Transportation (FAST'93), Japan, vol. 2, 1993, pp. 1231–1244.
[18] A. Molland, J. Wellicome, P. Couser, Resistance Experiments on a Systematic Series of High Speed Displacement Catamaran Forms: Variation of Length-Displacement Ratio and Breadth-Draught Ratio, University of Southampton, Department of Ship Science, Report No. 71, 1994, p. 82 + i.
[19] A. Molland, J. Wellicome, P. Couser, Theoretical Prediction of the Wave Resistance of Slender Hull Forms in Catamaran Configurations, University of Southampton, Department of Ship Science, Report No. 72, 1994, p. 24 + i.
[20] L. Doctors, The prediction of ship resistance by a blended theoretical and experimental method, in: Proc. 7th Int. Conference on Computational Methods and Experimental Measurements (CMEM'95), Italy, 1995, pp. 413–422.
[21] L. Doctors, A practical method of prediction of ship resistance for displacement vessels, in: Proc. 6th Int. Symposium on Practical Design of Ships and Mobile Units (PRADS'95), Society of Naval Architects of Korea, Korea, vol. 1, 1995, pp. 648–659.
[22] K. Hanhirova, S. Rintala, T. Karppinen, Preliminary resistance prediction method for fast mono- and multihull vessels, in: Proc. Int. Symposium on High Speed Vessels for Transport and Defence, Royal Institution of Naval Architects (RINA), England, vol. 6, 1995, pp. 1–17.
[23] P. Couser, An Investigation into the Performance of High-speed Catamarans in Calm Water and Waves, University of Southampton, Department of Ship Science, Doctoral Thesis, 1996, pp. 91–122.
[24] L. Doctors, A. Day, Resistance prediction for transom-stern vessels, in: Proc. 4th Int. Conference on Fast Sea Transportation (FAST'97), Australia, vol. 2, 1997, pp. 743–750.
[25] S. Robards, L. Doctors, Transom-hollow prediction for high-speed displacement vessels, in: Proc. 7th Int. Conference on Fast Sea Transportation (FAST'03), Italy, vol. 1A, 2003, pp. 19–26.
[26] L. Doctors, R. Beck, The separation of the flow past a transom stern, in: Proc. 1st Int. Conference on Marine Research and Transportation (ICMRT'05), Italy, 2005, p. 14.
[27] L. Doctors, C. McKesson, The Resistance Components of a Surface-effect Ship, the 26th Int. Symposium on Naval Hydrodynamics, Italy, 2006, pp. 1–15.
[28] L. Doctors, Investigation of the free-surface and resistance of transom-stern vessels, in: Proc. Pacific International Maritime Conference (PIMC'06), Australia, 2006, pp. 196–205.

[29] L. Doctors, Influence of the transom-hollow length on wave resistance, in: Proc. 21st Int. Workshop on Water Waves and Floating Bodies (IWWWFB'21), England, 2006, p. 4.
[30] E. Tuck, L. Luzauskas, D. Scullen, Sea Wave Pattern Evaluation. Part 1 Report: Primary Code and Test Results (Surface Vessels), Applied Mathematics Department, The University of Adelaide, 1999.
[31] P. Couser, J. Wellicome, A. Molland, An improved method for the theoretical prediction of the wave resistance of transom-stern hulls using a slender body approach, Int. Shipbuild. Prog. 45 (444) (1998).
[32] Skin friction and turbulence, in: Proc. 8th Int. Towing Tank Conference (ITTC'57), Madrid, 1957.
[33] Michlet©, Wave Resistance Prediction Software, 2010, <http://www.cyberiad.net>.
[34] T. Mynard, P. Sahoo, J. Mikkelsen, D. McGreer, Numerical and Experimental Study of Wave Resistance for Trimaran Hull Forms, Australian Maritime College, Australia, 2008, pp. 117–132.